

2D printed graphene conductive layers with high carrier mobility



Evgeniy Yakimchuk ^{a,*}, Regina Soots ^a, Igor Kotin ^a, Irina Antonova ^{a,b,c}

^a Rzhanov Institute of Semiconductor Physics SB RAS, 630090, Novosibirsk, 13 Lavrentyev Avenue, Russia

^b Novosibirsk State University, 630090, Novosibirsk, 2, Pirogov Street, Russia

^c Novosibirsk State Technical University, 630073, Novosibirsk, 20, K. Marxa pr, Russia

ARTICLE INFO

Article history:

Received 9 March 2017

Received in revised form

1 August 2017

Accepted 20 September 2017

Available online 21 September 2017

Keywords:

Graphene suspensions

Electrochemical exfoliation

Water-based inks

Printed layer electric properties

ABSTRACT

The comparison of different suspensions, obtained from the same material source subjected to electrochemical exfoliation and to analogous auxiliary treatments, but in different solutions, allowed choosing the most effective approach to obtaining graphene suspensions. It was found for the layers with a thickness of 10–20 nm printed from a water-based suspension that the sheet resistance was 5–10 kΩ/□, and the carrier mobility was equal to 30–40 cm²/V·s. The most important parameter determining the mobility of carriers in the films obtained from suspensions is found to be the flake thickness. The carrier mobility strongly decreased from ~100 to 0.05 cm²/V·s when the flake thickness changed from one monolayer to few monolayers (up to ~4–5 nm). This effect is most likely associated with the quality of the connection between the flakes. Only monolayer - bilayer flakes are capable of forming real connections in the film due to van-der-Waals forces.

© 2017 Elsevier B.V. All rights reserved.

1. Introduction

Due to the increasing number of materials used in printed electronics, it is becoming a universal platform for electronic industry, allowing one to create cheap, lightweight devices with a wide range of applications [1]. Printed technologies have several attractive features, such as direct (mask-free) patterning, purely additive operation, compatibility with traditional materials and scalability to large-area manufacturing [2]. Moreover, two-dimensional (2D) printed technologies serve as base for the development of flexible, foldable, wearable, transparent electronics [1–5].

2D layered materials, such as graphene and reduced graphene oxide due to their excellent mechanical properties, are widely used for conductive layers on flexible substrates. Graphene is known as a material which can sustain up to 25% in-plane tensile elastic strains. A strain applied to graphene can change its electronic structure and electric properties [6–8]. This theory was supported by experiments showing that the resistance of a graphene film transferred to a PDMS substrate isotropically stretched by 12% does not practically change, and significant resistivity changes start for a uniaxial stretching above 25% [9]. Generally, due to a unique combination of graphene properties (high carrier mobility, high thermal conductivity, transparency

in a wide range of wavelengths, etc., graphene-based printed layers are expected to be very promising in flexible and printed electronics [3]. Indeed, graphene and a reduced graphene oxide, due to their excellent mechanical properties, are widely used for conductive and functional layers in flexible devices. Among them are, for example, all-printed heterostructures biocompatible 2D crystal inks [10], the flexible graphene micro-transistors for brain activity mapping [11], ultrathin photodetector devices with graphene electrodes [12], enhanced performance of light-controlled conductive switching in hybrid cuprous oxide/reduced graphene oxide (Cu₂O/rGO) nanocomposites [13], 3D graphene nanostructures for the creation of low-cost and disposable graphene-based electrochemical electrodes for myriad applications including sensors, biosensors, fuel cells [14], etc.

One of the conductive film parameters, which is important for electronic applications, is carrier mobility in the printed films. The maximal carrier mobility values observed in the printed layers are 92–95 cm²/V·s [15,16]. On the other hand, the carrier mobility in the printed graphene or reduced graphene oxide layers is often very low (<1 cm²/V·s) [17–19].

In the present study we have not only found a promising approach to create a water-based graphene suspension for printed technologies but also compared the parameters of the films formed from a wide spectrum of suspensions created with the use of the known approaches (ethanol and propanol based liquid phase exfoliation). This comparison allows finding the main parameter determining the carrier mobility in the printed layers. Even when

* Corresponding author.

E-mail address: eyakimchuk@nsc.isp.ru (E. Yakimchuk).

we fabricated relatively thick printed layers (20–40 nm) the flake thickness had to be of 1–2 monolayers to provide a high carrier mobility in the printed layers to ensure a reliable connection between the flakes.

2. Experimental

A method for obtaining graphene-based ink by electrochemical exfoliation in the liquid phase in environmentally safe media, such as water (H₂O), isopropyl alcohol (IS) and the mixture of ethanol with water, followed by centrifugation and ultrasonic treatment is described in the present article. We have used the same highly oriented pyrolytic graphite (HOPG) as pristine materials, the same regime of electrochemical exfoliation and cleaning procedures, the same ultrasonic and centrifugation regimes for additional treatments. It allows us to compare the properties of suspensions and the layers created from these suspensions.

The electrochemical exfoliation of graphite occurred in the acid water solution and allowed obtaining flakes in a wide range of lateral sizes and thicknesses [20]. As the resulting material inherited the defects of the original substance, the carbon source was HOPG. The electrolyte, in which the cleavage occurred, was an acid solution (NH₄)₂S₂O₈ of 0.15 g per 100 ml of water.

After the electrochemical exfoliation of graphite the flakes dimensions lie in a wide range, and that is not suitable for their use in printing. The nanoparticles dispersed in the ink should be much smaller than the size of the printhead nozzle to prevent its clogging and blockage [15]. It is known that the lateral dimensions of the particles have to make up ~1/50 of the nozzle diameter (20 μm in our case), i.e., the flake size should be less than 400 nm. Therefore, to further reduce the flake size, the suspensions were additionally treated using ultrasound and centrifugation, which increase the efficiency of the presented method. It is important that the results obtained by the flakes electrochemical exfoliation contain a large number of intercalated gases, which greatly facilitates their subsequent exfoliation [4]. The ultrasonication of the suspensions was carried out on the setup with a capacity of 100 W for 24 h. Subsequent centrifugation occurred at 9000 revolutions per minute for 2 h. In the course of additional processing, the solution was added with surface active materials (surfactants) to improve the size reduction efficiency. The variation of surfactant concentration enabled a further investigation of the surfactants influence on the electric properties of the resulting graphene films. After obtaining the suspension the acid solution was replaced by water.

The suspension created as described above is further designated as G-1. In this work, we used three modified suspensions in which surfactants were added at different technological stages. As a result, three types of suspensions were obtained and designated as (G-1a, G-1b, G-1c); in them the surfactant at a concentration of ~0.01–0.02% was added at the final stages of centrifuging, in the middle of the technological process and in its initial phase, respectively. The surfactants addition at the initial stage of the suspension production was found to result in obtaining flakes with a thickness of 1–2 monolayers. In other cases the flake thickness was higher. The suspensions parameters are shown in Table 1.

The following suspensions were fabricated for comparison. G-2 is a suspension, obtained by exfoliation in an aqueous ethanol solution. In accordance with the data of work [21], two types of solutions with different exfoliation efficiencies were used (see Table 1). As expected, the thinnest (monolayer) particles were obtained in the solution when the ratio of ethanol and water was 70:30, however, in this case there was a significant number of flakes with a thickness of up to 3 nm. At the solution composition of 30:70 the major amount of particles had a thickness of ~1 nm. Suspension G-3 was obtained in isopropyl alcohol solution. In this case it is

Table 1

Suspension and layer description, graphene flakes (lateral size *l* and thickness *h*) parameters, films created by drops: resistivity ρ measured by 4-probe methods, and carrier mobility μ measured for transistor structures using a silicon substrate as a gate.

Suspension	Solution	<i>l</i> , nm	<i>h</i> , nm	ρ , k Ω/\square 4 probe	μ , cm ² /V·s
G-1a	H ₂ O + Surfactant	90–200	3–5	0.2–1.1	1.8
G-1b	H ₂ O + Surfactant	60–150	1–2	0.06–0.7	4.8
G-1c	H ₂ O + Surfactant	50–100	0.4–1.0	2.3–2.9	10–50
G-2a	Ethanol: H ₂ O (30:70)	130–140	~1	0.5–1.0	9
G-2b	Ethanol: H ₂ O (70:30)	80–300	0.4–3	8–12	32
G-3	IS	1000	5–20	45–120	0.02–0.3

known [22] that the exfoliation is not effective, and the thickness of the particles is rather large, i.e. 5–20 nm.

After all treatment processes the ready drops of suspensions were deposited on silicon substrates with 300 nm SiO₂ and annealed at a temperature of 60–120 °C for 1 h for drying, and the resulting film was used for further study of the structure, surface morphology and electrical properties. For electrical measurements on the surface the contacts using the silver paste were created.

A Solver PRO NT-MDT scanning microscope was used for obtaining Atomic force microscopy (AFM) images of the suspension flakes, film surfaces and for determining the film thickness. The measurements were performed in both contact and semi-contact modes. Raman spectra were recorded at room temperature, the excitation wavelength being 514.5 nm (2.41 eV argon ion laser). In order to avoid the heating of samples with laser emitted radiation, the laser beam power was decreased to 2–3 mW. Scanning electron microscopy (SEM) images were obtained using a JEOLJSM-7800F scanning electron microscope with the energy of primary electrons equal to 2 keV. Sheet resistance of the films was studied with the use of the four-probe JANDEL equipment and HM21 Test Unit. For measuring capacitance–voltage (C-V) and current–voltage (I-V) characteristics, an E7-20 immitancemeter and a Keithley picoamperemeter (model 6485) were used. The printer Dimatix FUJIFILM DMP-2831 was used for printing.

3. Experimental results

3.1. Structural properties: Raman spectroscopy

To study the structure of the obtained samples the Raman spectroscopy was used. Fig. 1 shows the Raman spectrum for the structure printed with graphene-based ink on a SiO₂/Si substrate. The peak positions detected on the spectra are as follows. D ~1350 cm⁻¹, G ~1580 cm⁻¹, G' (or D') ~1620 cm⁻¹, 2D ~2700 cm⁻¹, 2D' (or D + G) ~2940 cm⁻¹. The peak positions, in general, are characteristic of the suspensions, obtained by electrochemical exfoliation of graphite [23]. The G band have FWHM (full width at half maximum) values ~35 cm⁻¹.

D mode is related to defects in graphene [24], however, this does not mean that the exfoliated graphene contains defects of the plane, since the edges are also defects. In order to identify the quality of the flakes it is necessary to determine whether D mode is correlated with planar or edge defects, so at an increase in the frequency of the centrifuge rotation, the intensity of D peak increases, since the growth of the number of flakes increases the number of edge states. The ratio of intensities of the D/G peaks is known to be proportional to the inverse lateral size of the flakes [25].

Raman spectroscopy may be used to characterize the properties of graphene, such as the edge of the graphene flake. Due to the hexagonal structure of the graphene lattice, the ordered crystal

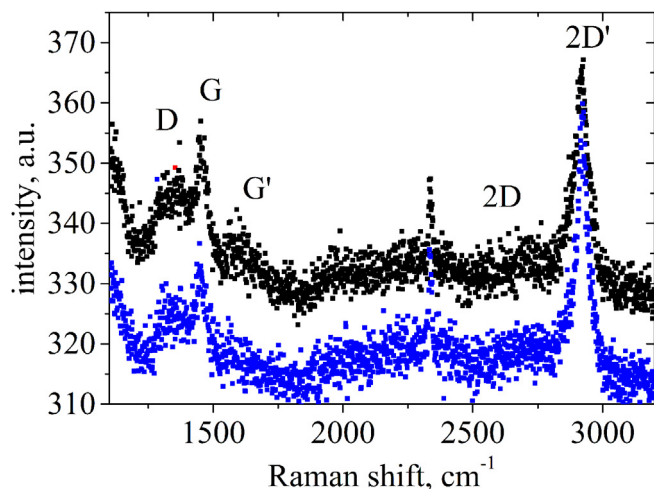


Fig. 1. Typical Raman spectra for layer printed with graphene inks G-1a with aqueous based composition. Different spectra correspond to various points on the printed layer. Layer thickness was 16 nm.

edges may have two basic structures: zigzag and armchair. However, only the edges of arm-chairs are capable of elastic scattering of charge carriers, which results in the appearance of a D band. It has been shown that a strong D band appears near the edges of the flakes of arm-chair type under polarized laser irradiation, directed along the edge line [26]. Therefore, it may be assumed that the weak intensity of the D band in our case is a case of dominance of the flakes of zigzag type in the bulk.

The nature of defects in graphene may be investigated by using the ratio of intensities of D and D' bands [7,27]. Compared to the above articles, the obtained correlations of peaks lie in the expected region for boundary effects. Thus, the defects that have a strong influence on the D peak, are the boundary conditions. The intensity of the 2D mode is also affected by defects, and with their increase the amplitude of the 2D band decreases [28].

It is known that the electrochemical exfoliation does not introduce additional defects, apart from the boundary ones. Thus the ultimate suspension inherits the defects of the source material, and in our case it was almost defect-free HOPG. This also proves the fact that our final suspensions have mostly edge defects.

The intensity of the 2D' band unexpectedly turned out to be dominant. The 2D' band have FWHM (full width at half maximum) values $\sim 53 \text{ cm}^{-1}$. The key to explain the brightness of the 2D band, and other overtone bands in Raman spectra is based on Kramers-Heisenberg-Dirac theory [29]. E. Heller demonstrates that transition sliding (sliding phonon production) explains graphene's extremely bright overtone 2D band, and in the case of small-flake graphene suspension the brightness of 2D' (or D + G) band with position $\sim 2940 \text{ cm}^{-1}$ also can be observed. Spectra of this type were found for the first time, and their interpretation requires additional research.

3.2. Structural properties: film morphology

Typical dimensions of flakes in the suspension, used for printing, were determined using atomic force microscope. AFM analysis of the suspension G-1c obtained in the acid aqueous solution (Fig. 2(a) and (b)) has shown that a significant part of flakes have a thickness of 1–3 monolayer (~ 0.4 – 1.0 nm). In general, the thickness of the flakes varied with low concentration within 3 nm. The lateral dimensions of the resulting flakes ranged from 50 to 400 nm. Adding a surfactant prior to centrifugation and ultrasonic

treatment allows improving the exfoliation efficiency, as the smallest flakes were obtained in this case.

The increase in surfactant concentration allowed reducing the characteristic thicknesses of the flakes, but, as it will be shown below, this led to an increase in the resistance of layers obtained from such a suspension.

The parameters of the suspensions obtained with the use of other solutions are also given in Table 1. The use of an aqueous solution of ethanol enabled obtaining suspensions G-2 with similar parameters as G-1. An aqueous solution of isopropyl alcohol (G-3) in this case did not lead to efficient exfoliation of the graphite.

3.3. Electrical properties of layers created from suspension

The sheet resistance of the films created from the suspension by drop casting, or by printing, was measured in two ways: with the four-probe method or the two contact one. The results obtained in different ways, well agreed with each other.

The resistance of the films fabricated from suspensions with different content of surfactant was compared. As a result, the sheet resistance of the film obtained from the suspension without surfactant was $3 \text{ k}\Omega/\square$, and after adding 0.17% surfactant the resistance increased to $31 \text{ k}\Omega/\square$. It is seen that substances stabilizing flakes and furthering their exfoliation to thinner ones, necessary for further use of suspensions as printing inks, reduce the conductivity of the suspensions.

Fig. 3(a) presents current – voltage characteristics of the layers obtained from different suspensions. It is seen that in all cases, these characteristics are linear. The resistances of the layers calculated from these characteristics are given in Table 1. The least resistance was $70 \text{ Ohm}/\square$, and was obtained in solution G-1b.

The carrier mobility was determined by the transfer characteristic of the transistor structure (Fig. 3(b) and (c)). As drain and source we used Ag contacts, and the gate was a low-resistivity silicon substrate with the gate dielectric of 300 nm SiO_2 . In order to estimate mobility transfer characteristics (drain–source current as the function of the gate voltage) were measured. A constant voltage of 100 mV was applied between the drain and the source, and the dependences of the drain current on the gate voltage were obtained. From transfer characteristics one can extract values of hole and electron mobilities calculated for linear parts of characteristic by the following formula:

$$\mu = \frac{L}{C_g W V_{DS}} \frac{\Delta I_{DS}}{\Delta V_g}, \quad (1)$$

where L is the transistor channel length; W is its width; C_g is the specific capacity of the gate dielectric; V_{DS} is the drain-source voltage; and ΔI_{DS} and ΔV_g are the increments of the drain current and the gate voltage, respectively. The best carrier mobility $\sim 50 \text{ cm}^2/\text{V}\cdot\text{s}$ for holes and electrons was obtained for the suspension G-1c.

The dependence of carrier mobility in the films created from different suspensions on the flakes thickness, presented in Fig. 4, shows that with a decrease in thickness the mobility increases. For the sake of completeness, Fig. 4 was added with the data Ref [15] for the case when monolayer particles dominate in the suspension (mobility of $95 \text{ cm}^2/\text{V}\cdot\text{s}$), and with carrier mobility for the films from suspensions, obtained by intercalation of *N*-methylpyrrolidone (NMP), Ref. [4].

It is also shown that the isochronous annealing of samples at $300 \text{ }^\circ\text{C}$ improves the conductivity by two orders of magnitude (Fig. 3(d)); this is due to the removal of surfactants and other impurities associated with the use of chemicals in the suspension production.

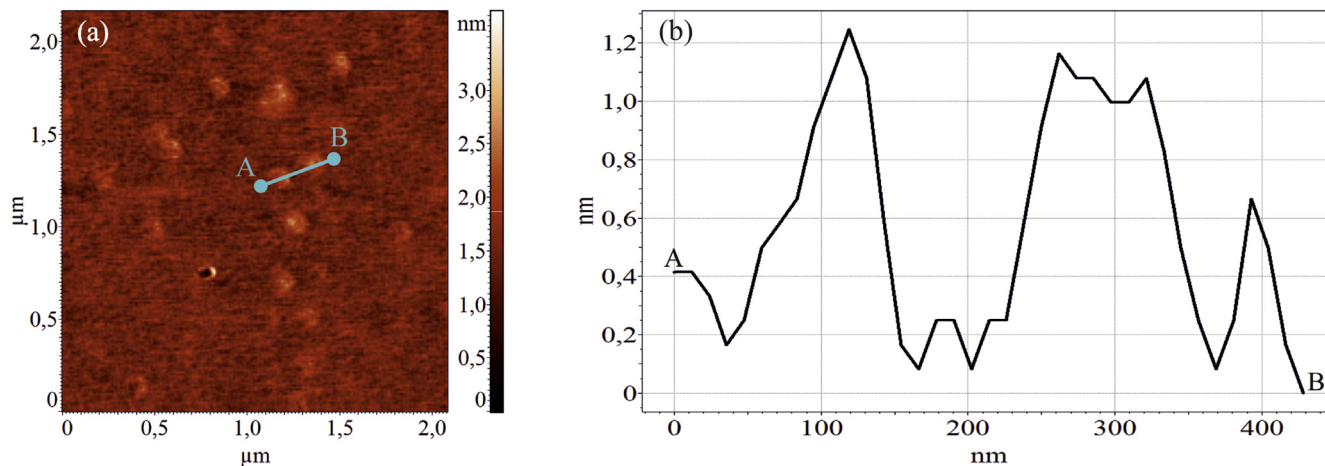


Fig. 2. (a) AFM image of the suspension flakes G-1c and (b) thickness profiles for the two flakes.

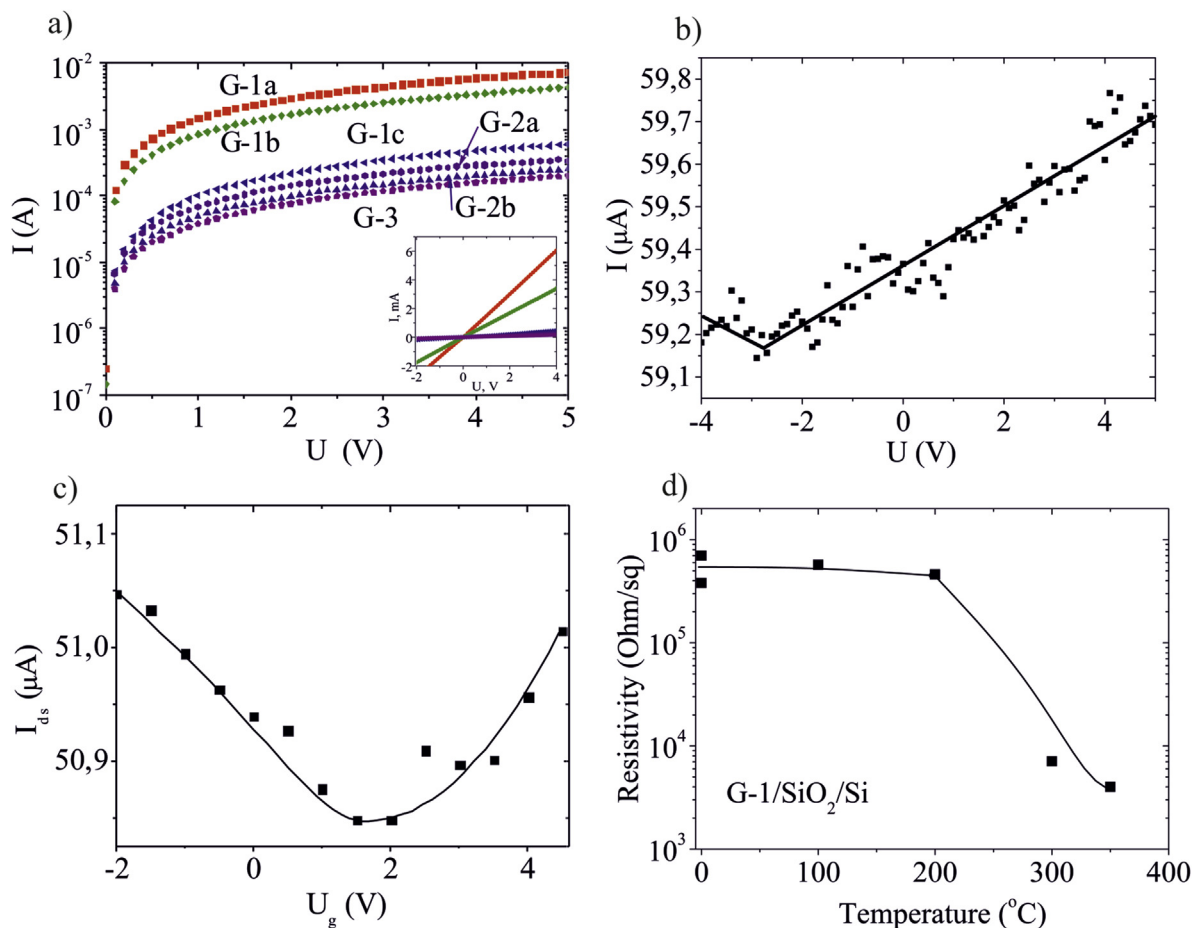


Fig. 3. (a) Lateral current – voltage characteristics for layers obtained from different suspensions and given in different scales ((a) gives the I-V in the logarithmic scale and Insert in the linear scale). (b,c) Transfer characteristics of transistor structures, obtained from the suspension G-1b, the mobility of electrons in this case amounted to $4.8 \text{ cm}^2/\text{V}\cdot\text{s}$, and the structure from suspensions of G-1c with the mobility of $\sim 51 \text{ cm}^2/\text{V}\cdot\text{s}$. (d) A change in the surface resistance of the film, obtained from the suspension G-1b after annealing.

3.4. The parameters of printed layers on rigid and flexible substrates

Suspensions G-1b were used for printing on a flexible substrate of polyethylene terephthalate (PET), paper and SiO_2/Si coated with a film of polyvinyl alcohol (PVA) to ensure the surface

hydrophilicity, which is necessary in printing with water-based inks (Fig. 5). The morphology of the film in Fig. 5(b) is associated with partial dissolution of the PVA film during printing. The used ink composition was slightly different from the one of G-1 suspensions. Ink of water based graphene should contain additives providing stability of solution and a certain combination of such

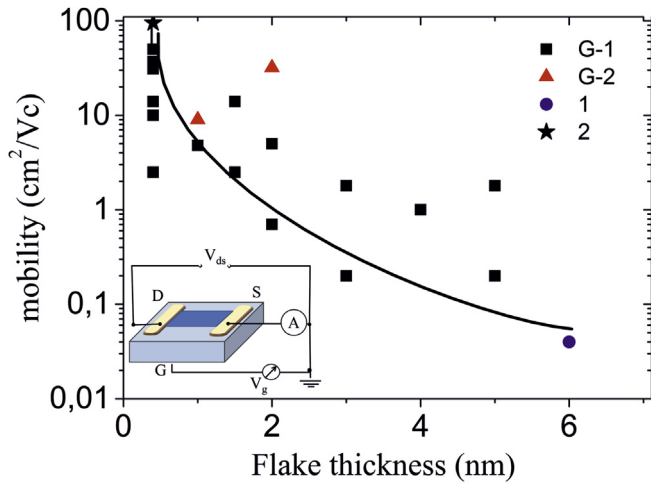


Fig. 4. The dependence of the carrier mobility in the films obtained from suspensions of different types. Points 1 and 2 correspond to the data from Refs. [4,15], respectively. Sketch of sample measurement is given in insert.

parameters as viscosity, surface tension, density, etc. to ensure the conditions for the formation of droplets during printing and solid films without coffee ring effect in drying. Fig. 5 demonstrates possible fabrication of thin continuous films using ink from the water-based suspension G-1b. The thickness of the printed films was 8–16 nm.

Fig. 6 shows images of the individual printed drops. For the drop

with a thickness of 2–3 nm, printed on the SiO₂/Si substrate and annealed at 350 °C for 20 min in inertial atmosphere, the contacts were made from silver paste, and I-V characteristics were measured. The measured sheet resistance of a thin printed film was 16 MΩ/□, which corresponds to resistivity of 4.8 Ω cm. The resistance of layers, printed on paper (Fig. 5(c)) was slightly higher 80 MΩ/□, and after annealing at 200°C (the maximum possible annealing temperature for paper) the resistance decreased to 700 kΩ/□ (resistivity of ~1.1 Ω cm). The relatively high resistance of layers printed on paper is due to low annealing temperature, and the effect of a high paper relief on the conductivity of the thin printed layer. The resistance of layers with a thickness of 15–20 nm on the SiO₂/Si substrate after annealing at 350 °C was already 5–10 kΩ/□ (resistivity of (0.8–1.6) × 10⁻² Ω cm). The carrier mobility measured for few structures at this last case was 30–40 cm²/V·s. For thick layers (100–200 nm) electrical properties of the water-based suspensions give the minimum resistance value of 200 Ω/□.

4. Discussion

Flakes and nanoparticles dispersed in the ink should be less than the size of the printhead nozzles to prevent clogging. In our case this means that the size should be less than 400 nm. On the other hand when reducing the lateral dimensions the number of joints between the flakes increases, and as a consequence the total loss in electrical properties increases. These contradictory conditions limit the resulting characteristics of the printed layers [15].

Electrochemical exfoliation of graphite in liquid phase allows obtaining graphene flakes with a thickness of up to one - two layers

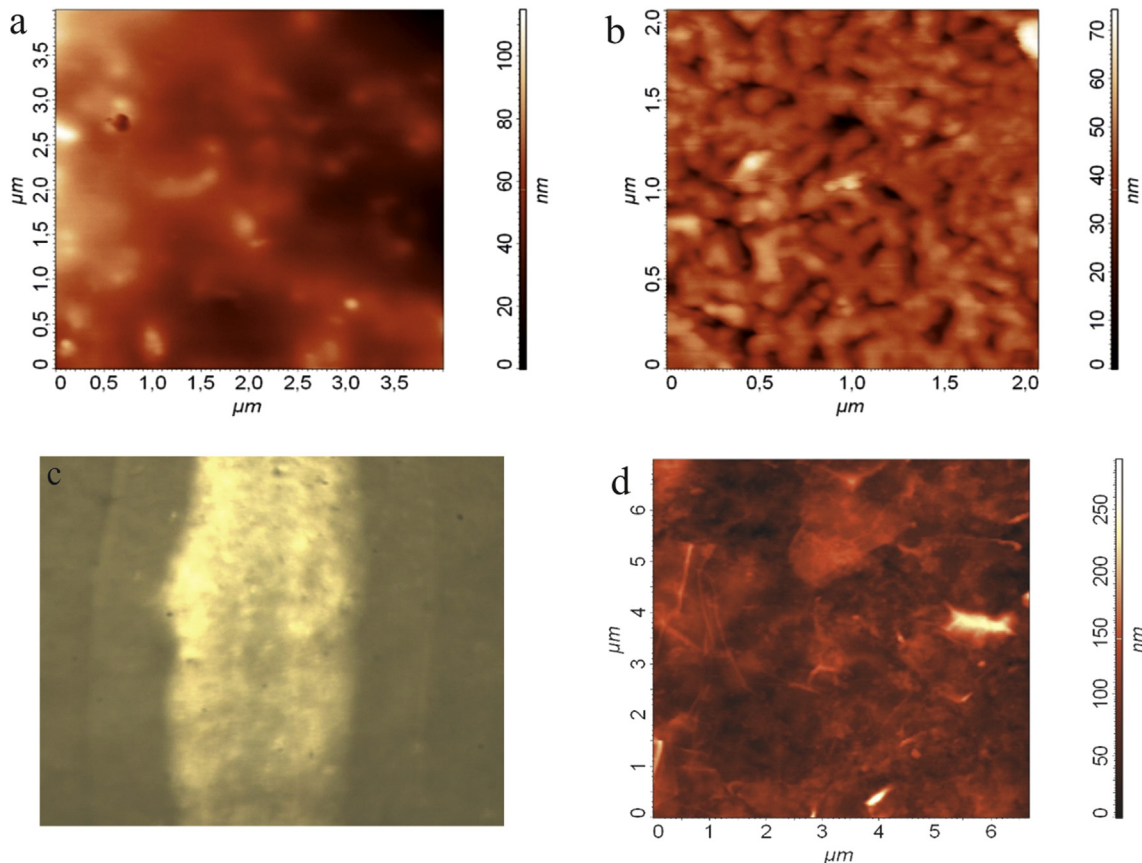


Fig. 5. (a) AFM images of graphene films with a thickness of 16 nm on PET substrates and (b) PVA - SiO₂/Si. (c) Optical and (d) AFM images of a graphene layer printed on paper. Thickness of the printed films ranged from 8 to 16 nm.

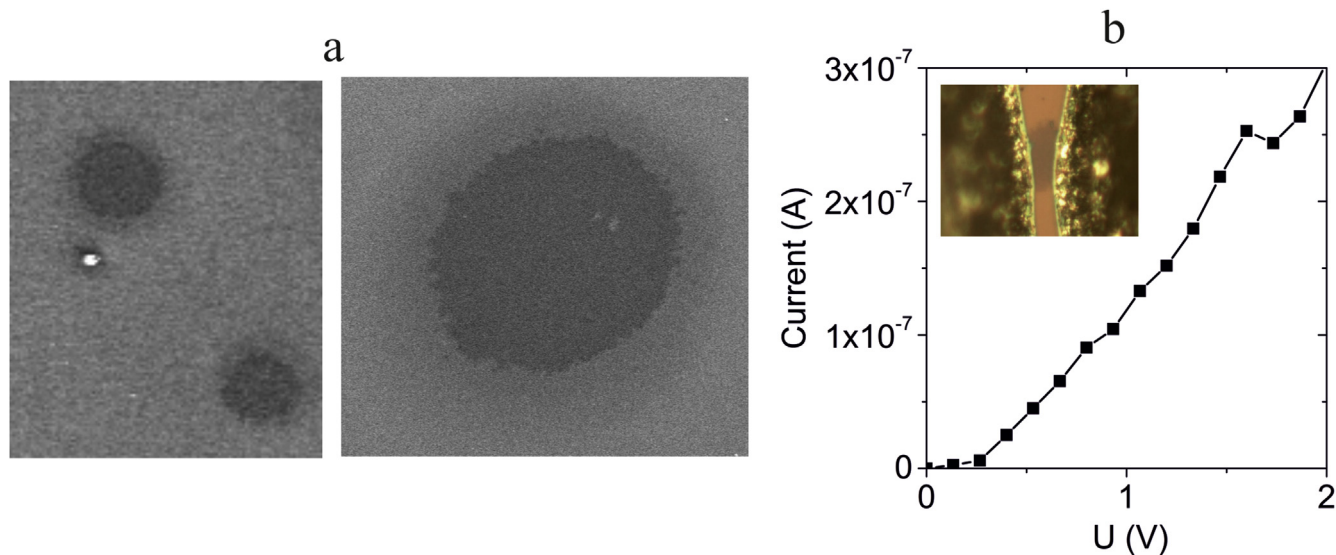


Fig. 6. (a) SEM images of individual printed drops (drop size $\sim 50 \mu\text{m}$) and (b) measurement of I-V characteristics on the drop with a thickness of $\sim 3 \text{ nm}$. The sheet resistance of the drop was $16 \text{ M}\Omega/\square$, which correspond to resistivity of $4.8 \Omega \text{ cm}$. Insert shows image of the drop with Ag contacts on the $300 \text{ nm SiO}_2/\text{Si}$ substrate.

and without oxidation. Earlier electrochemical exfoliation of graphite for subsequent ink production occurred in organic solvents with addition of extra stabilizing agents, which reduces initial electrical properties of graphene and adds unwanted contamination and impurities [30]. Electrochemical exfoliation does not introduce additional defects, therefore the quality of the final material depends on the initial substance. Variation in the solution for electrochemical exfoliation is known to leads to oxidation of the graphene flakes [31]. Relatively high conductivity of our suspension without annealing, and the Raman spectra with a narrow G peak demonstrated that, in our $(\text{NH}_4)_2\text{S}_2\text{O}_8$ solution, oxidation is not a pronounced process.

It is known that with the increasing layer thickness from graphene to graphite there is an increase in the specific resistivity of the material in the range from $1.0 \mu\Omega \text{ cm}$ [3,32] to $250\text{--}500 \mu\Omega \text{ cm}$ [33] and a decrease in the carrier mobility from $200\ 000\text{--}230\ 000 \text{ cm}^2/\text{V}\cdot\text{s}$ [34,35] at room temperature to $200 \text{ cm}^2/\text{V}\cdot\text{s}$ [36]. The mobility dependence on the thickness obtained theoretically predicts a 4–5 times decrease in carrier mobility in the transition from a monolayer to a layer thickness of $\sim 4 \text{ nm}$. The similar results were obtained in the theoretical and experimental study [37] where the decrease in carrier mobility was connected with the increase of the carrier mobility in thicker films. Experimentally, in the case of suspensions, we observed the range of $100\text{--}0.01 \text{ cm}^2/\text{V}\cdot\text{s}$ [4,15,38] for the same range of flakes thickness. The comparison of various suspensions properties, according to different publications, is difficult because of the changes in quite a large number of parameters. A similar approach applied in this study and using the same type of the original graphite and one type of surfactant, etc. allowed obtaining the experimental dependence of the carriers mobility in the films obtained from suspensions, depending on the flake suspension thickness. It turned out that this parameter largely determines the carriers mobility in the film: it varies in the range of $\sim 100\text{--}0.05 \text{ cm}^2/\text{V}\cdot\text{s}$ when the flakes thickness changes from 0.4 nm (monolayer) to several nanometers.

The carrier mobility in our film is limited by the disorder of each flake and the flake-to-flake junctions. The reason for sharp a decrease in the mobility observed in our study is, most likely, dependent on the quality of the connection between the flakes. The dominant effect of the flexibility for the properties of the films

created from the few-layer graphene flakes is observed in different aspects and, for instance, for the specific heat of the N-layer system [39]. Generally, as it is demonstrated in Fig. 4 and by Dhar [39] the properties depended on the flexibility decrease with the increase in flakes thickness $\sim N^{-1}$. As a result, only monolayer or bilayer flakes can form a film with good connections due to the excellent flexibility of such flakes. As a result, strong van-der-Waals forces appear only in the last case.

The results showed that to obtain relatively high carrier mobility in relatively thick (tens of nanometers) printed films there is a need in the suspension with flakes thickness of no more than 1–2 monolayers.

It should be also noted that the layer conductivity is largely determined not only by the thickness of flakes, but by a number of other parameters, in particular the amount of added surfactant, etc.

5. Conclusion

Comparison of different suspensions, obtained from the same source material subjected to electrochemical exfoliation and analogous auxiliary treatments, with the same surfactants, etc., but in different solutions, allowed choosing the most effective approach to obtain the suspensions. It turned out that the highest conductivity and mobility of charge carriers was detected in the films, obtained for water-based graphene suspensions. Moreover, the smallest flake thickness resulted from electrochemical exfoliation in water, followed by ultrasonic treatment. It were found for the layers with thickness of $15\text{--}20 \text{ nm}$ printed from this suspension on the SiO_2/Si substrate after annealing at $350 \text{ }^\circ\text{C}$ that sheet resistance was $5\text{--}10 \text{ k}\Omega/\square$ (resistivity of $(0.8\text{--}1.6) \times 10^{-2} \Omega \text{ cm}$), and the carrier mobility was $30\text{--}40 \text{ cm}^2/\text{V}\cdot\text{s}$. Inks based on a mixture of water and ethyl alcohol showed somewhat worse electrical properties of printed layers at treatments for the same time. The worst characteristics, as expected, appeared for films, printed with ink fabricated with use of isopropyl alcohol.

It was found that one of the most important parameter determining the mobility of carriers in the films obtained from suspensions is the flake thickness. The carrier mobility varies in the range $\sim 100\text{--}0.05 \text{ cm}^2/\text{V}\cdot\text{s}$ at flake thickness changing from 0.4 nm (monolayer) to several nanometers ($\sim 4\text{--}5 \text{ nm}$), which is most likely

associated with the quality of the connection between the flakes. Only monolayer - bilayer flakes are capable of forming fair connections in the film due to van der Waals forces.

Acknowledgements

The authors express their gratitude to V.B. Timofeev, from the Ammosov North-Eastern Federal University, for his assistance in the scanning electron microscopy measurements. This study was financially supported in part by the Russian Science Foundation (grant No. 15-12-00008).

References

- [1] A. Capasso, A.E. Del Rio Castillo, H. Sun, A. Ansaldò, V. Pellegrini, F. Bonaccorso, Ink-jet printing of graphene for flexible electronics: an environmentally-friendly approach, *Solid State Commun.* 224 (2015) 53–63.
- [2] J. Li, M.C. Lemme, M. Östling, Inkjet printing of 2D layered materials, *Chem-PhysChem.* 15 (2014) 3427–3434, <http://dx.doi.org/10.1002/cphc.201402103>.
- [3] A.K. Geim, K.S. Novoselov, The rise of graphene, *Nat. Mater.* 6 (2007) 183–191, <http://dx.doi.org/10.1038/nmat1849>.
- [4] R.A. Soots, E.A. Yakimchuk, N.A. Nebogatikova, I.A. Kotin, I. V Antonova, Graphene suspensions for 2D printing, *Tech. Phys. Lett.* 42 (2016) 438–441.
- [5] S. Majee, M. Song, S.-L. Zhang, Z.-B. Zhang, Scalable inkjet printing of shear-exfoliated graphene transparent conductive films, *Carbon N. Y.* 102 (2016) 51–57.
- [6] G. Cocco, E. Cadelano, L. Colombo, Gap opening in graphene by shear strain, *Phys. Rev. B - Condens. Matter Mater. Phys.* 81 (2010), <http://dx.doi.org/10.1103/PhysRevB.81.241412>.
- [7] J. Zhao, G.-Y. Zhang, D.-X. Shi, Review of graphene-based strain sensors, *Chin. Phys. B* 22 (2013) 57701, <http://dx.doi.org/10.1088/1674-1056/22/5/057701>.
- [8] S.-M. Choi, S.-H. Jhi, Y.-W. Son, Effects of strain on electronic properties of graphene, *Phys. Rev. B* 81 (2010) 81407, <http://dx.doi.org/10.1103/PhysRevB.81.081407>.
- [9] K.S. Kim, Y. Zhao, H. Jang, S.Y. Lee, J.M. Kim, K.S. Kim, J.-H. Ahn, P. Kim, J.-Y. Choi, B.H. Hong, Large-scale pattern growth of graphene films for stretchable transparent electrodes, *Nature* 457 (2009) 706–710, <http://dx.doi.org/10.1038/nature07719>.
- [10] D. McManus, S. Vranic, F. Withers, V. Sanchez-Romaguera, M. Macucci, H. Yang, R. Sorrentino, K. Parvez, S.-K. Son, G. Iannaccone, Water-based and biocompatible 2D crystal inks for all-inkjet-printed heterostructures, *Nat. Nanotechnol.* 12 (2017) 343–350.
- [11] B.M. Blaschke, N. Tort-Colet, A. Guimerà-Brunet, J. Weinert, L. Rousseau, A. Heimann, S. Drieschner, O. Kempki, R. Villa, M. V Sanchez-Vives, Mapping brain activity with flexible graphene micro-transistors, *2D Mater* 4 (2017) 25040.
- [12] H. Tan, Y. Fan, Y. Zhou, Q. Chen, W. Xu, J.H. Warner, Ultrathin 2D photodetectors utilizing chemical vapor deposition grown WS₂ with graphene electrodes, *ACS Nano* 10 (2016) 7866–7873.
- [13] J. Wei, Z. Zang, Y. Zhang, M. Wang, J. Du, X. Tang, Enhanced performance of light-controlled conductive switching in hybrid cuprous oxide/reduced graphene oxide (Cu₂O/rGO) nanocomposites, *Opt. Lett.* 42 (2017) 911–914.
- [14] S.R. Das, Q. Nian, A.A. Cargill, J.A. Hondred, S. Ding, M. Saei, G.J. Cheng, J.C. Claussen, 3D nanostructured inkjet printed graphene via UV-pulsed laser irradiation enables paper-based electronics and electrochemical devices, *Nanoscale* 8 (2016) 15870–15879, <http://dx.doi.org/10.1039/C6NR04310K>.
- [15] F. Torrisi, T. Hasan, W. Wu, Z. Sun, A. Lombardo, T.S. Kulmala, G.W. Hsieh, S. Jung, F. Bonaccorso, P.J. Paul, D. Chu, A.C. Ferrari, Inkjet-printed graphene electronics, *ACS Nano* 6 (2012) 2992–3006, <http://dx.doi.org/10.1021/nn2044609>.
- [16] S. Wang, P.K. Ang, Z. Wang, A.L.L. Tang, J.T.L. Thong, K.P. Loh, High mobility, printable, and solution-processed graphene electronics, *Nano Lett.* 10 (2010) 92–98, <http://dx.doi.org/10.1021/nl9028736>.
- [17] S. Wang, P.J. Chia, L.L. Chua, L.H. Zhao, R.Q. Png, S. Sivaramakrishnan, M. Zhou, R.G.S. Goh, R.H. Friend, A.T.S. Wee, P.K.H. Ho, Band-like transport in surface-functionalized highly solution-processable graphene nanosheets, *Adv. Mater.* 20 (2008) 3440–3446, <http://dx.doi.org/10.1002/adma.200800279>.
- [18] J. Li, F. Ye, S. Vaziri, M. Muhammed, M.C. Lemme, M. Östling, Efficient inkjet printing of graphene, *Adv. Mater.* 25 (2013) 3985–3992, <http://dx.doi.org/10.1002/adma.201300361>.
- [19] Y. Su, S. Jia, J. Du, J. Yuan, C. Liu, W. Ren, H. Cheng, Direct writing of graphene patterns and devices on graphene oxide films by inkjet reduction, *Nano Res.* 8 (2015) 3954–3962, <http://dx.doi.org/10.1007/s12274-015-0897-5>.
- [20] K. Parvez, Z.-S. Wu, R. Li, X. Liu, R. Graf, X. Feng, K. Müllen, Exfoliation of graphite into graphene in aqueous solutions of inorganic salts, *J. Am. Chem. Soc.* 136 (2014) 6083–6091.
- [21] W.-W. Liu, B.-Y. Xia, X.-X. Wang, J.-N. Wang, Exfoliation and dispersion of graphene in ethanol-water mixtures, *Front. Mater. Sci.* 6 (2012) 176–182.
- [22] U. Halim, C.R. Zheng, Y. Chen, Z. Lin, S. Jiang, R. Cheng, Y. Huang, X. Duan, A rational design of cosolvent exfoliation of layered materials by directly probing liquid–solid interaction, *Nat. Commun.* 4 (2013) 2213, <http://dx.doi.org/10.1038/ncomms3213>.
- [23] K.R. Paton, E. Varrla, C. Backes, R.J. Smith, U. Khan, A. O'Neill, C. Boland, M. Lotya, O.M. Istrate, P. King, T. Higgins, S. Barwich, P. May, P. Puczkarski, I. Ahmed, M. Moebius, H. Pettersson, E. Long, J. Coelho, S.E. O'Brien, E.K. McGuire, B.M. Sanchez, G.S. Duesberg, N. McEvoy, T.J. Pennycook, C. Downing, A. Crossley, V. Nicolosi, J.N. Coleman, Scalable production of large quantities of defect-free few-layer graphene by shear exfoliation in liquids, *Nat. Mater.* 13 (2014) 624–630, <http://dx.doi.org/10.1038/nmat3944>.
- [24] A.C. Ferrari, J.C. Meyer, V. Scardaci, C. Casiraghi, M. Lazzeri, F. Mauri, S. Piscanec, D. Jiang, K.S. Novoselov, S. Roth, A.K. Geim, Raman spectrum of graphene and graphene layers, *Phys. Rev. Lett.* 97 (2006), <http://dx.doi.org/10.1103/PhysRevLett.97.187401>.
- [25] U. Khan, A. O'Neill, M. Lotya, S. De, J.N. Coleman, High-concentration solvent exfoliation of graphene, *Small* 6 (2010) 864–871, <http://dx.doi.org/10.1002/sml.200902066>.
- [26] Y. You, Z. Ni, T. Yu, Z. Shen, Edge chirality determination of graphene by Raman spectroscopy, *Appl. Phys. Lett.* 93 (2008), <http://dx.doi.org/10.1063/1.3005599>.
- [27] A. Eckmann, A. Felten, A. Mishchenko, L. Britnell, R. Krupke, K.S. Novoselov, C. Casiraghi, Probing the nature of defects in graphene by Raman spectroscopy, *Nano Lett.* 12 (2012) 3925–3930.
- [28] I. Childres, L.A. Jauregui, J. Tian, Y.P. Chen, Effect of oxygen plasma etching on graphene studied using Raman spectroscopy and electronic transport measurements, *New J. Phys.* 13 (2011) 25008.
- [29] E.J. Heller, Y. Yang, L. Kocia, W. Chen, S. Fang, M. Borunda, E. Kaxiras, Theory of graphene Raman scattering, *ACS Nano* 10 (2016) 2803–2818, <http://dx.doi.org/10.1021/acsnano.5b07676>.
- [30] A. Ciesielski, P. Samorì, Graphene via sonication assisted liquid-phase exfoliation, *Chem. Soc. Rev.* 43 (2014) 381–398, <http://dx.doi.org/10.1039/c3cs60217f>.
- [31] A. Ambrosi, M. Pumera, Electrochemically exfoliated graphene and graphene oxide for energy storage and electrochemistry applications, *Chem. A Eur. J.* 22 (2016) 153–159, <http://dx.doi.org/10.1002/chem.201503110>.
- [32] C. Berger, Z. Song, X. Li, X. Wu, N. Brown, C. Naud, D. Mayou, T. Li, J. Hass, A.N. Marchenkov, E.H. Conrad, P.N. First, W.A. de Heer, Electronic confinement and coherence in patterned epitaxial graphene, *Science* (80-.) 312 (2006) 1191–1196, <http://dx.doi.org/10.1126/science.1125925>.
- [33] H.O. Pierson, Handbook of Carbon, Graphite, Diamonds and Fullerenes: Processing, Properties and Applications (Materials Science and Process Technology), 1993, <http://dx.doi.org/10.1016/B978-0-8155-1339-1.50008-6>.
- [34] K.I. Bolotin, K.J. Sikes, Z. Jiang, M. Klima, G. Fudenberg, J. Hone, P. Kim, H.L. Stormer, Ultrahigh electron mobility in suspended graphene, *Solid State Commun.* 146 (2008) 351–355, <http://dx.doi.org/10.1016/j.ssc.2008.02.024>.
- [35] K.I. Bolotin, K.J. Sikes, J. Hone, H.L. Stormer, P. Kim, Temperature-dependent transport in suspended graphene, *Phys. Rev. Lett.* 101 (2008), <http://dx.doi.org/10.1103/PhysRevLett.101.096802>.
- [36] X.-Y. Fang, X.-X. Yu, H.-M. Zheng, H.-B. Jin, L. Wang, M.-S. Cao, Temperature- and thickness-dependent electrical conductivity of few-layer graphene and graphene nanosheets, *Phys. Lett. A* 379 (2015) 2245–2251.
- [37] K. Nagashio, T. Nishimura, K. Kita, A. Toriumi, Mobility variations in mono- and multi-layer graphene films, *Appl. Phys. Express* 2 (2009) 25003, <http://dx.doi.org/10.1143/APEX.2.025003>.
- [38] A.C. Arias, S.E. Ready, R. Lujan, W.S. Wong, K.E. Paul, A. Salleo, M.L. Chabinyr, R. Apte, R.A. Street, Y. Wu, P. Liu, B. Ong, All jet-printed polymer thin-film transistor active-matrix backplanes, *Appl. Phys. Lett.* 85 (2004) 3304–3306, <http://dx.doi.org/10.1063/1.1801673>.
- [39] S. Dhar, A.R. Barman, G.X. Ni, X. Wang, X.F. Xu, Y. Zheng, S. Tripathy, Ariando, A. Rusydi, K.P. Loh, M. Rubhausen, A.H.C. Neto, B. Zylimaz, T. Venkatesan, A new route to graphene layers by selective laser ablation, *AIP Adv.* 1 (2011) 22109, <http://dx.doi.org/10.1063/1.3584204>.